How Does Helium Get into Buckminsterfullerene?

Serguei Patchkovskii and Walter Thiel*

Contribution from the Organisch-chemisches Institut, Universität Zürich, Winterthurerstrasse 190, CH-8057 Zürich, Switzerland

Received March 11, 1996[⊗]

Abstract: Reaction mechanisms for helium incorporation into C_{60} have been examined by semiempirical (MNDO), *ab initio* (HF/3-21G), and density functional (BLYP/3-21G, BP86/3-21G) calculations. Effective activation barriers for the penetration through an intact cage and for the insertion through the two possible one-bond windows and six different two-bond windows are reported both in the lowest singlet and triplet state. The computed barriers are very high and exceed 200 kcal/mol for each of the 21 pathways considered. These results require a new mechanistic interpretation of the high-pressure experiments where helium incorporation into fullerenes is observed under thermal conditions. Mechanistic alternatives are discussed including the possible role of imperfect C_{60} isomers and other intermediates.

1. Introduction

Endohedral fullerene complexes[1−3] with a noble gas inside the fullerene cage have first been detected in mass-spectroscopic collision experiments.[4−6] For example, colliding high-energy (8 keV) C_{60}^+ ions with a He target gas yields He@C_{60}^+, which can be neutralized to He@C_{60}.[7] Such complexes can also be prepared thermally by heating a fullerene in a noble gas atmosphere,[8] preferably under high pressure,[9] with typical yields of e.g. He@C_{60} around 0.1% after 5 h at 600 °C and 2500 atm.[9,10] Incorporation of ^{3}He allows the detection of ^{3}He NMR spectra[10] which may be used as a powerful tool for following chemistry on the surface of the fullerenes.[11,12] The insertion of Ne, Ar, Kr, and traces of Xe has also been observed in the high-pressure experiments.[9]

Theoretical calculations predict very high barriers for the direct passage of He through a hexagon of carbon atoms, e.g. 11.5 (C_{60}, MNDO),[13] 10.7 (C_6H_6, *ab initio* MP2),[14] or 9.35 eV (C_{60}, model potential)[15] for the neutral species, and slightly lower values for the cations.[13,14] In the collision experiments,[1,4−7] there is enough kinetic energy available to overcome such barriers. The observed threshold energy for endohedral He@C_{60} formation under single-collision conditions depends strongly on the internal energy of the fullerene.[16] It amounts to 8 ± 1 eV for cold C_{60}^- anions and decreases both for C_{60}^+ and C_{60}^- with increasing internal energy.[16] Collisions between Ne^+ and C_{60} require a threshold energy of at least 20 eV for producing the endohedral Ne@C_{60}^+ complex.[17]

The thermal insertion reactions[8−12] in the high-pressure experiments must proceed along pathways with much lower barriers. The measured temperature dependence for the release of He from He@C_{60} indicates a barrier around 80 kcal/mol.[8] To account for these observations, a window mechanism has been proposed[8] where one or more bonds are broken reversibly to open a temporary "window" in the cage allowing easy incorporation of guests, with a possible involvement of triplet states through intersystem crossing. Recently, window formation in the first excited triplet state has also been implied in the breakdown of fullerene cages upon ultraviolet laser irradiation.[18]

Theoretical evidence for the window mechanism is provided by quantum-chemical calculations[19] on window-type structures in C_{60} (MNDO) and in a corannulene model system (MNDO, *ab initio* SCF, DFT). Scans of the triplet potential surfaces suggest that such structures with one broken bond are local minima. In the case of C_{60}, this minimum lies about 3.0 eV above the triplet fullerene, and the barrier to reach it from the singlet ground state is estimated to be 5.2 eV. These computational results[19] support the window mechanism, but they suffer from three limitations: First, the passage of helium through the window has not been treated and is thus implicitly assumed to have a negligible barrier, which is not self-evident. Second, the higher-level methods have been applied only to the corannulene model system, but not to C_{60}. Third, the unrestricted Hartree−Fock (UHF) method has been employed for the triplet states in spite of possible problems with spin contamination (see below).

The present paper reports a comprehensive theoretical study of the mechanism of He incorporation into C_{60} which is not

[⊗] Abstract published in *Advance ACS Abstracts,* July 1, 1996.

(1) Schwarz, H.; Weiske, T.; Böhme, D. K.; Hrušák, J. In *Buckminsterfullerenes*; Billups, W. E., Cuifolini, M. A., Eds.; VCH: New York, 1993; pp 257−283.
(2) Bethune, D. S.; Johnson, R. D.; Salem, J. R.; de Vries, M. S.; Yannoni, C. S. *Nature* **1993**, *366*, 123−128.
(3) Cioslowski, J. *Electronic Structure Calculations on Fullerenes and Their Derivatives*; Oxford University Press: Oxford, 1995; pp 176−213.
(4) Weiske, T.; Böhme, D. K.; Hrušák, J.; Krätschmer, W.; Schwarz, H. *Angew. Chem., Int. Ed. Engl.* **1991**, *30*, 884−886.
(5) Ross, M. M.; Callahan, J. H. *J. Phys. Chem.* **1991**, *95*, 5720−5723.
(6) Caldwell, K. A.; Giblin, D. E.; Hsu, C. S.; Cox, D.; Gross, M. L. *J. Am. Chem. Soc.* **1991**, *113*, 8519−8521.
(7) Weiske, T.; Wong, T.; Krätschmer, W.; Terlouw, J. K.; Schwarz, H. *Angew. Chem., Int. Ed. Engl.* **1992**, *31*, 183−185.
(8) Saunders, M.; Jiménez-Vázquez, H. A.; Cross, R. J.; Poreda, R. J. *Science* **1993**, *259*, 1428−1430.
(9) Saunders, M.; Jiménez-Vázquez, H. A.; Cross, R. J.; Mroczkowski, S.; Gross, M. L.; Giblin, D. E.; Poreda, R. J. *J. Am. Chem. Soc.* **1994**, *116*, 2193−2194.
(10) Saunders, M.; Jiménez-Vázquez, H. A.; Cross, R. J.; Mroczkowski, S.; Freedberg, D. I.; Anet, F. A. L. *Nature* **1994**, *367*, 256−258.
(11) Saunders, M.; Jiménez-Vázquez, H. A.; Cross, R. J.; Billups, E.; Gesenberg, C.; McCord, D. J. *Tetrahedron Lett.* **1994**, *35*, 3869−3872.
(12) Saunders, M.; Jiménez-Vázquez, H. A.; Bangerter, B. W.; Cross, R. J.; Mroczkowski, S.; Freedberg, D. I.; Anet, F. A. L. *J. Am. Chem. Soc.* **1994**, *116*, 3621−3622.
(13) Kolb, M.; Thiel, W. *J. Comp. Chem.* **1993**, *14*, 37−44.
(14) Hrušák, J.; Böhme, D. K.; Weiske, T.; Schwarz, H. *Chem. Phys. Lett.* **1992**, *193*, 97−100.
(15) Mowrey, R. C.; Ross, M. M.; Callahan, J. H. *J. Phys. Chem.* **1992**, *96*, 4755−4761.
(16) Sprang, H.; Mahlkow, A.; Campbell, E. E. B. *Chem. Phys. Lett.* **1994**, *227*, 91−97.
(17) Wan, Z.; Christian, J. F.; Anderson, S. L. *J. Chem. Phys.* **1992**, *96*, 3344−3347.
(18) Juha, L.; Hamplová, V.; Engst, P.; Kubát, P.; Koudoumas, E.; Couris, S. *J. Phys. Chem.* **1995**, *99*, 8200−8201.
(19) Murry, R. L.; Scuseria, G. E. *Science* **1994**, *263*, 791−793.

S0002-7863(96)00769-X CCC: $12.00 © 1996 American Chemical Society

subject to these limitations. The passage of helium through a benzene ring is re-investigated (at higher theoretical levels than before[13,14]) to validate the methods employed. Mechanisms considered for C_{60} include the direct penetration of helium through the hexagons and pentagons of an intact cage, the formation of the two possible one-bond windows and six different two-bond windows, and the insertion of helium through such windows, both in the singlet and in the triplet state. The role of imperfect non-fullerene C_{60} structures and other mechanistic alternatives are also addressed.

2. Computational Methods

The fullerene calculations employed three computational levels: MNDO with standard parameters,[13,20] *ab initio* self-consistent-field (SCF) theory using the 3-21G basis set,[21] and density functional theory (DFT)[22] also using the 3-21G basis set. In the DFT calculations, the standard local functional[23] was augmented by nonlocal corrections for exchange[24] and correlation[25] (BLYP). The BLYP functional has been established to be quite accurate for a wide range of molecules,[26−28] but it seems to fail for the C_{20} isomers.[29,30] Therefore, additional test calculations were performed using the BP86 functional with a different nonlocal correction for correlation.[31] The BP86 results were generally similar to the BLYP results and thus will not be discussed separately.

In the MNDO calculations, the molecular geometries were fully optimized and characterized as minima or transition states by force constant analysis. Single-point energy calculations at the optimized MNDO structures were carried out at the *ab initio* SCF, BLYP, and BP86 levels. In addition, *ab initio* SCF and BLYP geometries were determined for all energy minima by optimizations starting from the corresponding MNDO structures.

As in previous theoretical work,[19] singlet states were described by closed-shell wave functions (MNDO, *ab initio*, DFT). Single-point MNDO calculations were performed to ensure that restricted open-shell singlet wave functions (two unpaired electrons, half-electron approximation[32]) do not yield lower energies than in the closed-shell case. This was found to be true for all relevant species on the singlet potential surface (MNDO).

Triplet states may be represented by restricted[32,33] or unrestricted[34] open-shell wave functions. The latter choice is legitimate only if spin contamination is negligible, i.e. if the S^2 expectation value is close to 2 for a triplet. As illustrated by the data in Table 1, this condition is satisfied only for the DFT calculations (UBLYP, UBP86), but not for the MNDO and *ab initio* SCF calculations (UHF) which is consistent with previous experience.[35] Hence, as a general rule, an unrestricted treatment for triplet states was applied only at the DFT level, whereas a restricted open-shell Hartree−Fock (ROHF) treatment was chosen at the MNDO level[32] and the *ab initio* level,[33] in contrast to previous work.[19] Inspection of Table 1 shows that this choice is essential because the UHF approach yields unreliable energies in the case of severe spin contamination: There is a spurious MNDO UHF solution for the singlet ground state of C_{60} (with symmetry breaking), and both the MNDO and *ab initio* (3-21G) UHF calculations predict triplet energies below the corresponding closed-shell ground-state energies of C_{60}. For comparison, the ROHF approach yields reasonable singlet−triplet splittings (MNDO 52 kcal/mol, *ab initio* 3-21G 61 kcal/mol) which are slightly above the available experimental values[36,37] (36−39 kcal/mol) and the present DFT results (34 kcal/mol for both UBLYP and UBP86).

Table 1. Results for the Lowest Singlet and Triplet States of C_{60}

label[a]	point group[b]	method[c]	S^2	ΔE[d]
1s	I_h	RHF/MNDO	0.0000	0.0[g]
	I_h	UHF/MNDO//RHF/MNDO[e]	8.2511	−43.9
	C_1	UHF/MNDO[e]	10.2847	−56.7
	I_h	RHF/3-21G	0.0000	0.0[h]
	I_h	RHF/3-21G//RHF/MNDO[f]	0.0000	33.1
	I_h	RBLYP/3-21G	0.0000	0.0[i]
	I_h	RBLYP/3-21G//RHF/MNDO[f]	0.0000	0.4
	I_h	RBP86/3-21G	0.0000	0.0[j]
	I_h	RBP86/3-21G//RHF/MNDO[f]	0.0000	1.7
1t	C_s	ROHF/MNDO	2.0000	52.4
	C_s	UHF/MNDO//ROHF/MNDO	10.1819	−23.2
	C_1	UHF/MNDO	11.9133	−40.2
	C_s	ROHF/3-21G	2.0000	60.5
	C_s	ROHF/3-21G//ROHF/MNDO	2.0000	100.1
	C_s	UHF/3-21G	8.7060	−13.7
	C_s	UHF/3-21G//ROHF/MNDO	8.6656	10.2
	C_s	UBLYP/3-21G	2.0027	34.1
	C_s	UBLYP/3-21G//ROHF/MNDO	2.0039	39.2
	C_s	UBP86/3-21G	2.0028	34.2
	C_s	UBP86/3-21G//ROHF/MNDO	2.0041	40.2

[a] s = singlet, t = triplet. [b] Symmetry enforced by the geometry specification. [c] Notation see text. A//B denotes an energy at level A computed using a geometry from level B. [d] Energy (kcal/mol) relative to the corresponding singlet ground-state energy from a spin-restricted calculation with geometry optimization. [e] Using a spin-polarized initial guess. [f] A spin-unrestricted calculation with a spin-polarized initial guess yields the spin-restricted solution. [g] Calculated heat of formation 869.3 kcal/mol. [h] Total energy −2259.04767 au. [i] Total energy −2272.76132 au. [j] Total energy −2273.62619 au.

The reference calculations for C_6H_6He employed a correlation-consistent polarized triple-ζ basis (cc-pVTZ)[38] where the set of basis functions with the highest angular momentum was omitted for each element. The contraction scheme for this basis (cc-pVTZ′) was (10s5p2d)/[4s3p2d] for C, (5s2p)/[3s2p] for H, and (6s2p)/[3s2p] for He, which led to 201 contracted functions for C_6H_6He. Electron correlation was treated at the *ab initio* levels of second-order Møller−Plesset perturbation theory (MP2)[39] and coupled-cluster theory with single and double excitations augmented by a perturbational treatment of connected triple excitations (CCSD(T)).[40,41]

The semiempirical calculations were performed using a modified MNDO94 program[42] with analytical derivatives of the half-electron ROHF energy.[43] The *ab initio* and DFT calculations made use of the Gaussian 92/DFT[44] and Gaussian 94[45] programs, with the exception of the CCSD(T) calculations, which were handled by MOLPRO94.[46]

(20) Dewar, M. J. S.; Thiel, W. *J. Am. Chem. Soc.* **1977**, *99*, 4899−4907, 4907−4917.
(21) Hehre, W. J.; Radom, L.; Schleyer, P.v.R.; Pople, J. A. *Ab Initio Molecular Orbital Theory*; Wiley: New York, 1986.
(22) Parr, R. G.; Yang, W. *Density-Functional Theory of Atoms and Molecules*; Oxford University Press: Oxford, 1989.
(23) Vosko, S. H.; Wilk, L.; Nusair, M. *Can. J. Phys.* **1980**, *58*, 1200−1211.
(24) Becke, A. D. *Phys. Rev. A* **1988**, *38*, 3098−3100.
(25) Lee, C.; Yang, W.; Parr, R. G. *Phys. Rev. B* **1988**, *37*, 785−789.
(26) Gill, P. M. W.; Johnson, B. G.; Pople, J. A. *Int J. Quantum Chem.* **1992**, *S26*, 319−331.
(27) Johnson, B. G.; Gill, P. M. W.; Pople, J. A. *J. Chem. Phys.* **1993**, *98*, 5612−5626.
(28) Wong, M. W.; Radom, L. *J. Phys. Chem.* **1995**, *99*, 8582−8588.
(29) Raghavachari, K.; Trucks, G. W.; Pople, J. A.; Head-Gordon, M. *Chem. Phys. Lett.* **1993**, *214*, 357−361.
(30) Taylor, P. R.; Bylaska, E.; Weave, J. H.; Kawai, R. *Chem. Phys. Lett.* **1995**, *235*, 558−563.
(31) Perdew, J. P. *Phys. Rev. B* **1986**, *33*, 8822−8824; **1986**, *34*, 7406.
(32) Dewar, M. J. S.; Trinajstic, N. *Chem. Commun.* **1970**, 646−647.
(33) Roothaan, C. C. J. *Rev. Mod. Phys.* **1960**, *32*, 179−185.
(34) Pople, J. A.; Nesbet, R. K. *J. Chem. Phys.* **1954**, *22*, 571−572.
(35) Baker, J.; Scheiner, A.; Andzelm, J. *Chem. Phys. Lett.* **1993**, *216*, 380−388.
(36) Hung, R. R.; Grabowski, J. J. *J. Phys. Chem.* **1991**, *95*, 6073−6075.
(37) Haufler, R. E.; Wang, L. S.; Chibante, L. P. F.; Jin, C.; Conceicao, J.; Chai, Y.; Smalley, R. E. *Chem. Phys. Lett.* **1991**, *179*, 449−454.
(38) Dunning, T. H. *J. Chem. Phys.* **1989**, *90*, 1007−1023.
(39) Møller, C.; Plesset, M. S. *Phys. Rev.* **1934**, *46*, 618−622.
(40) Purvis, G. D.; Bartlett, R. J. *J. Chem. Phys.* **1982**, *76*, 1910−1918.
(41) Raghavachari, K.; Trucks, G. W.; Pople, J. A.; Head-Gordon, M. *Chem. Phys. Lett.* **1989**, *157*, 479−483.
(42) Thiel, W. Program MNDO94, version 4.0, 1994.
(43) Patchkovskii, S.; Thiel, W. *Theor. Chim. Acta* **1996**, *93*, 87−99.

Table 2. Results for the Passage of Helium through Benzene[a]

method[b]	symm[c]	N_{imag}[d]	ΔE	R_{CC}	R_{CHe}
RHF/MNDO[e]	D_{3h}	1	293.0	1.481, 1.553	1.517
RHF/3-21G//RHF/MNDO	D_{3h}		284.6		
BLYP/3-21G//RHF/MNDO	D_{3h}		248.1		
BP86/3-21G//RHF/MNDO	D_{3h}		247.0		
RHF/MNDO	D_{6h}	2	293.1	1.515	
RHF/3-21G//RHF/MNDO	D_{6h}		284.7		
BLYP/3-21G//RHF/MNDO	D_{6h}		247.8		
BP86/3-21G//RHF/MNDO	D_{6h}		246.5		
RHF/3-21G	D_{3h}	1	286.7	1.443, 1.613	1.529
RHF/3-21G	D_{6h}	2	287.1	1.517	
BLYP/3-21G	D_{6h}	1	244.2	1.552	
BP86/3-21G	D_{6h}	1	243.5	1.548	
MP2/3-21G[f]	D_{3h}		258	1.554, 1.557	1.555
MP2/6-31G**//MP2/3-21G[f]	D_{3h}		247		
RHF/cc-pVTZ′	D_{6h}	1	269.6	1.500	
BLYP/cc-VTZ′	D_{6h}	1	236.1	1.529	
BP86/cc-VTZ′	D_{6h}	1	233.6	1.523	
MP2/cc-pVTZ′	D_{6h}	1	242.0	1.517	
BLYP/cc-pVTZ′//MP2/cc-pVTZ′	D_{6h}		236.2		
BP86/cc-pVTZ′//MP2/cc-pVTZ′	D_{6h}		233.6		
CCSD(T)/cc-pVTZ′//MP2/cc-pVTZ′	D_{6h}		239.9		

[a] Barriers ΔE (kcal/mol) and selected distances R_{AB} (Å) in the transition structure. [b] See text. cc-pVTZ′ denotes a cc-pVTZ basis without f functions at C and without d functions at H and He. [c] Point group symmetry. [d] Number of imaginary frequencies. [e] Reference 13. [f] Reference 14.

3. Results

Table 2 summarizes the reference calculations for the passage of helium through a benzene ring. This reaction proceeds via a planar transition structure with helium at the center of the ring. MNDO and *ab initio* RHF/3-21G computations predict a D_{3h} transition structure with CC bond alternation, but a second-order D_{6h} saddle point is only slightly higher in energy (by 0.1 and 0.4 kcal/mol, respectively) indicating a very flexible ring. The D_{6h} structure represents the genuine transition state at the BLYP/3-21G and BP86/3-21G levels as well as in all cc-pVTZ′ calculations (RHF, BLYP, BP86, MP2). The geometry of the D_{6h} structure is reproduced well by MNDO (cf. R_{CC} in Table 2, MNDO 1.515 Å vs MP2/cc-pVTZ′ 1.517 Å).

The most reliable barrier in Table 2 (CCSD(T)/cc-pVTZ′//MP2/cc-pVTZ′) amounts to 240 kcal/mol (10.4 eV) and is thus somewhat lower than the best previous theoretical estimate of 247 kcal/mol.[14] In the fullerene calculations (see below), the highest theoretical level for barriers involves BLYP/3-21G and BP86/3-21G energy evaluations at MNDO optimized geometries. According to Table 2, the corresponding barriers in the C_6H_6He case are lowered by 3−4 kcal/mol (1−2%) when reoptimizing all geometries at the DFT level, and by another 8−10 kcal/mol (3−4%) when using a polarized triple-ζ basis (cc-pVTZ′ instead of 3-21G). Compared with the best CCSD(T) barrier in Table 2, the BLYP/3-21G//RHF/MNDO and BP86/3-21G//RHF/MNDO values are too high by 6−8 kcal/mol (2−3%). Errors of similar magnitude may be expected in the fullerene calculations.

Table 3 lists theoretical relative energies for all isomeric structures **1**−**12** considered presently (s = singlet, t = triplet, see also Figure 1). Table 4 reports relative energies for the corresponding $C_{60}He$ transition structures **13**−**26** which are shown in Figures 2−5 using three orthogonal coordinate projections, with left and right structures being top and left views of the structure in the middle. Figures 1−5 depict the MNDO optimized geometries of the lowest-energy spin state of **2**−**26** (singlet or triplet).

Insertion of helium into an intact C_{60} cage should proceed in the singlet though one of the hexagons (via **13s**). Our best computed barrier is 229 kcal/mol (BLYP//MNDO), which may be corrected on the basis of the C_6H_6He results (see above) to yield a best estimate of 221 kcal/mol. This value is similar to the barrier from a model potential[15] and somewhat higher than the threshold energy in He + C_{60}^- collisions (8 ± 1 eV, 184 ± 23 kcal/mol).[16] The latter deviation is as expected since the insertion barriers are known to be smaller in the cations compared with the neutral molecules[13,14] which should also hold for the anions.

Direct insertion of the helium into singlet C_{60} through one of the pentagons (via **14s**) requires much more activation since **14s** lies ca. 100 kcal/mol above **13s** at all theoretical levels applied. The corresponding transition states on the triplet surface (**13t**, **14t**) are significantly higher in energy than their singlet counterparts (**13s**, **14s**) and show unsymmetrical (C_1) geometries.

Considering window mechanisms, only two types of one-bond windows are possible in buckminsterfullerene due to its high symmetry.[19] A 5−6 window is formed by breaking a bond shared by a pentagon and a hexagon, whereas a 6−6 window is generated by breaking a bond shared by two hexagons (see **2** and **3**, respectively, in Figure 1). Extending similar previous work,[19] sections of the MNDO potential surface corresponding to the opening of these windows are shown in Figure 6.

In the singlet state, stretching the C−C bond in both windows causes the relative heat of formation to increase sharply up to

(44) Frisch, M. J.; Trucks, G. W.; Schlegel, H. B.; Gill, P. M. W.; Johnson, B. G.; Wong, M. W.; Foresman, J. B.; Robb, M. A.; Head-Gordon, M.; Replogle, E. S.; Gomperts, R.; Andres, J. L.; Raghavachari, K.; Binkley, J. S.; Gonzalez, C.; Martin, R. L.; Fox, D. J.; Defrees, D. J.; Baker, J.; Stewart, J. J. P.; Pople, J. A. *Gaussian 92/DFT, Revision F.2*; Gaussian, Inc.: Pittsburgh, PA, 1993.

(45) Frisch, M. J.; Trucks, G. W.; Schlegel, H. B.; Gill, P. M. W.; Johnson, B. G.; Robb, M. A.; Cheeseman, J. R.; Keith, T.; Petersson, G. A.; Montgomery, J. A.; Raghavachari, K.; Al-Laham, M. A.; Zakrzewski, V. G.; Ortiz, J. V.; Foresman, J. B.; Peng, C. Y.; Ayala, P. Y.; Chen, W.; Wong, M. W.; Andres, J. L.; Replogle, E. S.; Gomperts, R.; Martin, R. L.; Fox, D. J.; Binkley, J. S.; Defrees, D. J.; Baker, J.; Stewart, J. P.; Head-Gordon, M.; Gonzalez, C.; Pople, J. A. *Gaussian 94, Revision B.3*; Gaussian, Inc.: Pittsburgh, PA, 1995.

(46) MOLPRO94 is a package of ab initio programs written by H. J. Werner and P. J. Knowles with contributions from J. Almlöf, R. D. Amos, M. J. O. Deegan, S. T. Elbert, C. Hampel, W. Meyer, K. A. Peterson, R. M. Pitzer, A. J. Stone, and P. R. Taylor.

Table 3. Relative Energies[a] (kcal/mol) for Isomeric C_{60} Structures

label[b]	point group[c]	MNDO[d]	RHF//MNDO[e]	BLYP//MNDO[e]	BP86//MNDO[e]	RHF[f]	BLYP[f]	remarks
1s	I_h	0.0	0.0	0.0	0.0	0.0	0.0	
1t	C_s	51.4	67.0	38.8	38.6	60.5	34.1	lowest triplet excitation
				Windows with a Single Bond Broken				
2s	C_s	[162.3][g]	[221.5]	[151.7]	[155.9]	*h*	*h*	5−6 bond open
2t	C_s	[123.2][i]	[142.9]	[148.0]	[151.4]	*h*	*h*	
3s	C_s	[159.0][g]	[205.6]	[141.7]	[145.8]	*h*	*h*	6−6 bond open
				Windows with Two Bonds Broken				
4s	C_s	157.7	172.0	169.8	176.6	169.3	164.9	adjacent bonds in pentagon open
4t	C_s	184.9	183.8	210.3	220.6	178.6	*h*	
5t	C_s	194.3	205.0	199.3	208.3	196.8	*h*	nonadjacent bonds in pentagon open
6s	C_1	156.7	168.3	160.3	166.2	166.3	156.6	adjacent bonds in hexagon open
6t	C_1	174.2	178.0	174.1	179.8	171.9	169.3	
7t	C_s	184.4	191.4	187.8	196.4	184.5	*h*	two 5−6 bonds in hexagon open
8s	C_s	284.7	305.9	274.4[j]	*k*	*h*	*h*	two 6−6 bonds in hexagon open
8t	C_s	269.7	286.4	267.6	278.4	*h*	*h*	
9t	C_s	254.8	325.6	251.8	262.3	*h*	*h*	para bonds in hexagon open
				Imperfect Structures				
10s	C_1	161.6	196.1	155.7	161.1	193.3	150.4	7- and 9-membered rings
10t	C_1	169.7	192.4	159.5	164.5	182.4	155.7	
11s	C_1	169.0	198.4	162.1	168.3	195.4	157.3	10-membered ring
11t	C_1	195.5	232.6[j]	185.1	191.2	230.0	178.1	
12s	C_1	188.2	249.3	209.1	216.7	247.5	202.8	8- and 10-membered rings
12t	C_1	216.7	271.0	233.3	240.8	257.8	224.0	

[a] Energies relative to the I_h C_{60} structure at the same level of approximation. [b] s = singlet, t = triplet. [c] Symmetry enforced by the geometry specification, actual symmetry may be higher. [d] Unless noted otherwise, all MNDO structures are true minima according to vibrational analysis. [e] Single-point calculations at the optimized MNDO geometry. [f] Calculations with geometry optimization. [g] Point of minimal gradient, see text. [h] Geometry optimization converges either to **1s** or **1t**. [i] Not a stationary point, see text. [j] Level shift method was used to enforce convergence. [k] No SCF convergence.

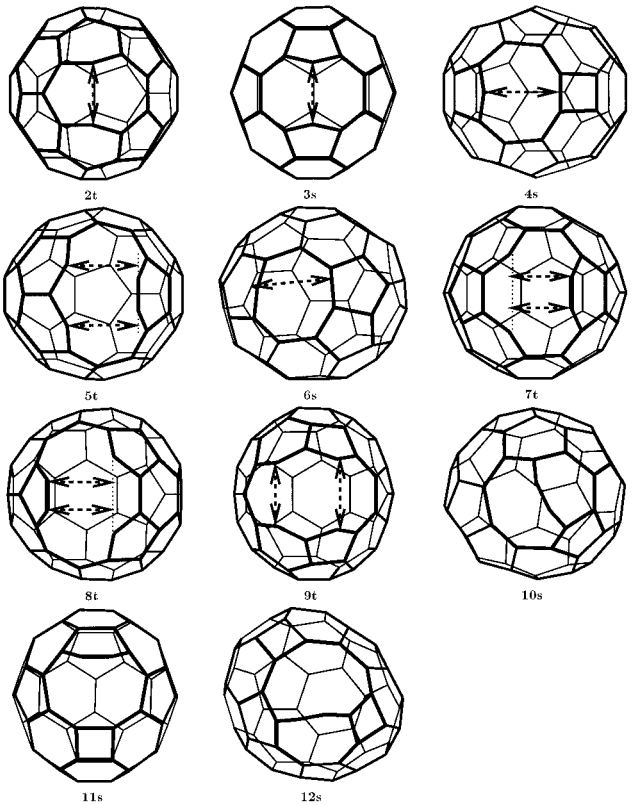

Figure 1. Minimum MNDO structures for the lowest-energy spin states of one- and two-bond windows and imperfect C_{60} isomers. Reaction coordinates used for opening the windows are indicated by the dashed arrows.

about 160 kcal/mol. After that point (achieved at a C−C separation of 2.84 Å for the 5−6 window and at 2.48 Å for the 6−6 window), the bond is practically broken. Opening a formed window further up to approximately 3.3 Å does not significantly increase the heat of formation. However, neither the 5−6 nor the 6−6 singlet window corresponds to a local minimum on the MNDO potential energy surface. The entries in Table 3 (**2s**, **3s**) correspond to the points of minimum gradient norm on the singlet curves in Figure 6, with C−C separations of 2.88 Å for the 5−6 window (**2s**) and 2.56 Å for the 6−6 window (**3s**). Geometry optimizations starting from these points (MNDO, *ab initio* RHF, BLYP) converge to the I_h structure **1s**, which makes the existence of stable 5−6 and 6−6 one-bond windows on the singlet surface unlikely.

In the triplet state, no local minimum is found for the 6−6 window (**3t**) up to a C−C separation of 3.3 Å. For the 5−6 window (**2t**) there is a flat region on the potential surface (see Figure 6) which seems to be separated from the fullerene (**1t**) by a small barrier and which appears to have a shallow minimum at a C−C distance of 2.6 Å. However, tracking this minimum is complicated by the existence of several MNDO SCF solutions involving spatially different π-type molecular orbitals of similar energy, which causes difficulties (discontinuities) in the geometry optimizations. We decided against investing the effort to locate these minima precisely, for two reasons: First, from a mechanistic point of view, it is more relevant to find the actual transition state for helium insertion through such a window (see below). Second, *ab initio* RHF and BLYP geometry optimizations starting from the approximate MNDO geometry for **2t** (C−C 2.6 Å) eventually yield the fullerene (**1t**) which casts some doubt on the existence of a genuine minimum. Therefore, the entry for **2t** in Table 3 is meant to characterize a flat "window-like" section on the triplet surface through a representative point.

Transition structures for the passage of helium through 5−6 and 6−6 windows have been located and fully characterized at the MNDO level, both on the singlet and triplet surface (cf. **15s**, **15t**, **16s**, **16t** in Table 4, see also Figure 2). Given the preceding remarks on window-type structures (**2s**, **2t**, **3s**, **3t**) it is clear that the effective barriers for these processes must refer

Table 4. Relative Energies[a] (kcal/mol) for the $C_{60}He$ Transition Structures

label[b]	point group[c]	MNDO[d]	RHF//MNDO[e]	BLYP//MNDO[e]	BP86//MNDO[e]	remarks
			Insertion into the Intact Cage			
13s	C_{3v}	265.0	266.6	229.0	228.0[f]	through a hexagon in **1**
13t	C_1	302.2	293.2	262.4	261.7	
14s	C_{5v}	359.5	375.5	327.8	328.3	through a pentagon in **1**
14t	C_1	413.3	446.0	371.6	372.2	
			Insertion through a One-Bond Window			
15s	C_s	259.2	274.3	252.0[i]	253.8[i]	through the 5−6 window in **2**
15t	C_1	246.8	256.8	239.8[f]	242.6	
16s	C_s	236.6	240.1	235.2	241.5	through the 6−6 window in **3**
16t	C_1	248.5	242.3	241.3	245.6	
			Insertion through a Two-Bond Window			
17s	C_s	247.5	240.3	228.9	235.5	through the window in **4**
17t	C_s	291.3	297.1	264.9	271.4	
18s	C_s	293.5	340.1	259.1	270.0	through the window in **5**
18t	C_s	253.6	274.3	259.4	269.5	
19s	C_1	304.6	322.5	*g*	*g*	through the window in **6** with bond breaking
19t	C_1	270.8	266.2	272.5[j]	283.8	
20s	C_1	280.1	267.6	246.0	251.3	through the window in **6**
20t	C_1	293.8	269.4	257.8	262.9	
21s	C_s	294.2	327.0	238.5	247.3	through the window in **7**
21t	C_s	244.7	256.8	242.7	251.7	
22s	C_s	325.7	353.9	322.1	336.6	through the window in **8**
22t	C_1	[341.2][h]	340.5	[317.8][i,k]	[330.6][i,l]	
23t	C_s	298.7	305.3	[306.4][f,m]	[316.7][n]	through the window in **9**
			Insertion through the Largest Ring in Imperfect Structures			
24s	C_1	255.5	267.5	215.1	219.7	through the 9-membered ring in **10**
24t	C_1	262.4	261.4	216.8	220.9	
25s	C_1	240.2	251.4	204.2	209.7	through the 10-membered ring in **11**
25t	C_1	264.3	279.5	224.0	229.4	
26s	C_1	242.9	282.1	234.6	241.8	through the 10-membered ring in **12**
26t	C_1	269.7	301.3	258.5	265.7	

[a] Energies relative to I_h C_{60} with He at infinite distance, computed at the same level of approximation. For **13**−**23**, the relative energies are equal to the effective activation barriers, see text. [b] s = singlet, t = triplet. [c] Symmetry enforced by the geometry specification, actual symmetry may be higher. [d] Unless noted otherwise, all MNDO structures are first-order saddle points according to vibrational analysis. [e] Single-point calculation at the optimized MNDO geometry. [f] Level shift method was used to enforce convergence. [g] No SCF convergence. [h] Second-order saddle point. First imaginary frequency (327i cm^{-1}) corresponds to the motion of He along the reaction coordinate. Second imaginary frequency (208i cm^{-1}) corresponds to the motion of He perpendicular to the window slit in **8t** (see Figure 1). [i] Quadratically convergent SCF procedure[56] used to enforce convergence. [j] $S^2 = 2.13$. [k] $S^2 = 2.28$ [l] $S^2 = 2.31$. [m] $S^2 = 2.66$. [n] $S^2 = 2.75$.

to the ground state fullerene (**1s**). These barriers are of the order of 240 kcal/mol at all theoretical levels (i.e. for **15t**, **16s**, **16t**, and even somewhat higher for **15s**). More than 90 kcal/mol (BLYP//MNDO, BP86//MNDO) are required for putting helium through the opening in a window-type structure such as **2t** (cf. **15t** in Table 4). This invalidates previous implicit assumptions[19] and would seem to rule out a one-bond window mechanism for helium insertion into C_{60}.

Considering two-bond windows which have been suggested as a likely alternative,[19] a complete study is not feasible since the number of symmetry-distinct pairs of bonds is quite large in C_{60}. Therefore, we consider only six different two-bond windows which correspond to the mechanistically interesting case of breaking two bonds in the same hexagon or the same pentagon to generate large holes in the cage (see **4**−**9** in Figure 1). Figure 7 illustrates the opening of these two-bond windows by following reaction coordinates which conserve all symmetry elements common to the I_h structure and the window structure being formed. Since this requires breaking two bonds simultaneously, the profiles on Figure 7 are expected to overestimate the barriers, but they provide reasonable starting structures for geometry optimizations.

From the 12 two-bond window structures considered (6 singlets and 6 triplets), only 9 correspond to local minima on the MNDO surface. Three of these (**8s**, **8t**, and **9t**) are very shallow and collapse to the fullerene (**1s** or **1t**) during geometry optimization at the *ab initio* RHF or BLYP level. Three others (**4t**, **5t**, and **7t**) converge to local minima at the *ab initio* RHF level, but collapse to **1t** with BLYP. Hence, there remain only three rather stable two-bond window structures (**4s**, **6s**, and **6t**). Among these, **4s** and **6s** are formed by breaking adjacent bonds in pentagons and hexagons, respectively, but the disrupted ring closes again to form a four- or five-membered ring, so that **4s** and **6s** have only one formal bond less than the I_h fullerene (**1s**). Incidentally, **6s** is identical to one of the "closed stick" structures,[47] proposed as a likely intermediate in C_{60} fragmentation and annealing processes.

Thirteen transition structures for the insertion of helium through two-bond windows of the types **4**−**9** (see Figure 1) have been found and fully characterized by force constant analysis at the MNDO level (cf. **17**−**23** in Table 4, see also Figures 3 and 4). These transition structures are generally in a one-to-one relation to the singlets and triplets of **4**−**9**, with the following exceptions: There are two paths for helium insertion through **6**. The first path (via **19s** and **19t**) involves breaking the newly formed five-membered ring in **6** and is favored on the triplet MNDO surface, whereas the second one (via **20s** and **20t**) retains the five-membered ring and is preferred in the singlet state. On the other hand, it was not possible to locate a transition state (**23s**) for helium passage through **9s** since the corresponding optimizations converged to **13s**, **14s**, or **16s**, for a range of reasonable starting geometries.

Relative to the ground state singlet fullerene (**1s**), the calculated energies for the transition states **17**−**23** are very high,

(47) Murry, R. L.; Strout, D. L.; Odom, G. K.; Scuseria, G. E. *Nature* **1993**, *366*, 665−667.

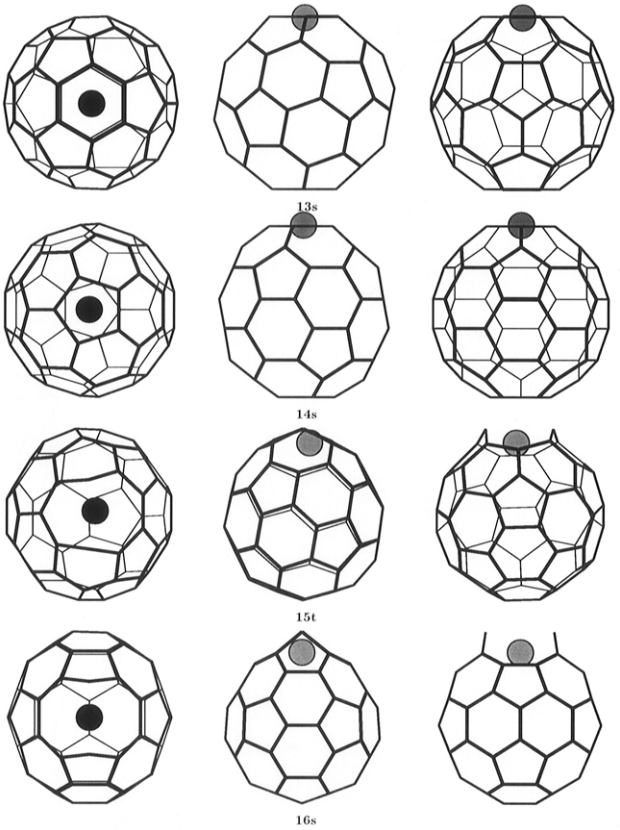

Figure 2. MNDO transition structures for direct He insertion into C_{60} (**13s**, **14s**) and for He passage through one-bond windows (**15t**, **16s**). Three orthogonal coordinate projections are given.

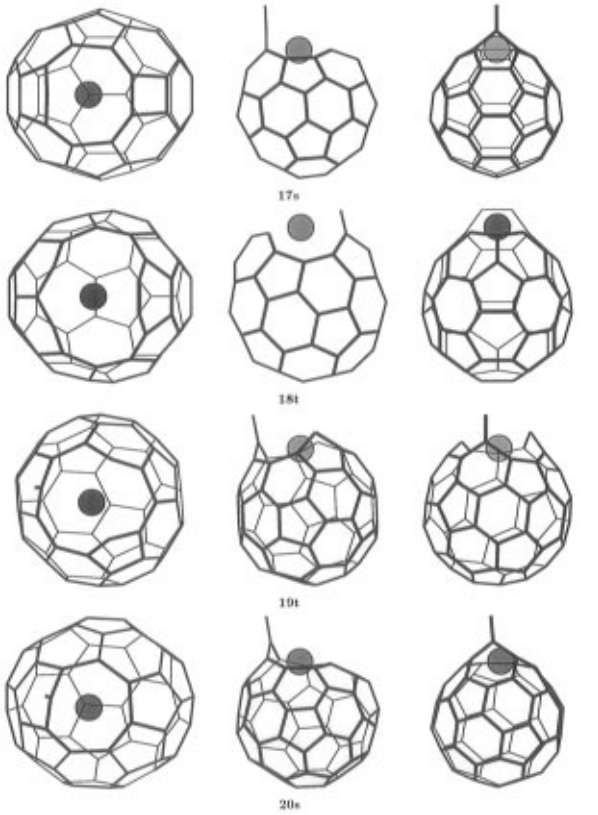

Figure 3. MNDO transition structures for He passage through two-bond windows (**17s**, **18t**, **19t**, **20s**). Three orthogonal coordinate projections are given.

i.e. above 225 kcal/mol at the BLYP//MNDO level and even above 240 kcal/mol in the MNDO and *ab initio* RHF calcula-

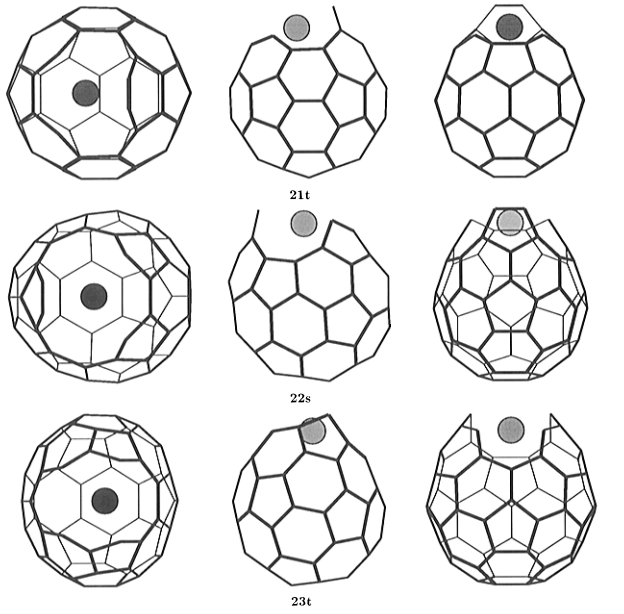

Figure 4. MNDO transition structures for He passage through two-bond windows (**21t**, **22s**, **23t**). Three orthogonal coordinate projections are given.

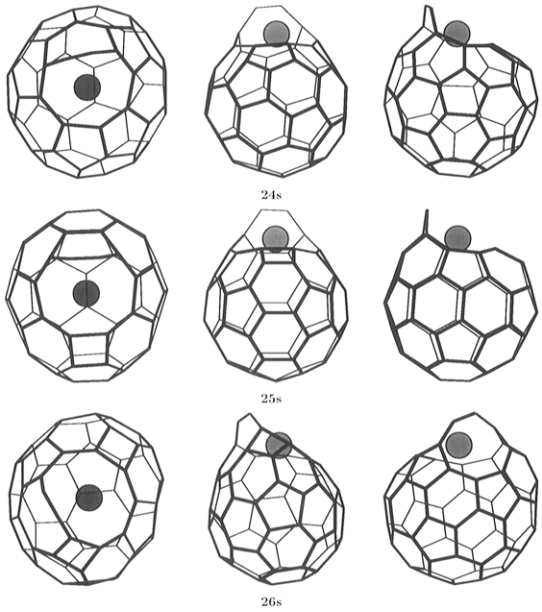

Figure 5. MNDO transition structures for He insertion into three imperfect structures (**24s**, **25s**, **26s**). Three orthogonal coordinate projections are given.

tions. These values represent the effective barriers for the two-bond window mechanisms, because any of the stable two-bond window structures (e.g. **4s**, **6s**, or **6t**, see above) are expected to exist in equilibrium with **1s** under the thermal conditions of the high-pressure experiments. It should be noted in this context that the barriers for helium insertion through a two-bond window are consistently higher than those for its closure to the fullerene (cf. the MNDO data in Table 4 and Figure 7).

Surveying the theoretical evidence available at this point, it is striking that all mechanisms considered require extremely high activation energies well above 200 kcal/mol. On the C_{60}He singlet surface, the lowest computed barriers for direct insertion (via **13s**), the one-bond window mechanism (via **16s**), and the two-bond window pathway (via **17s**) are 229, 235, and 229 kcal/mol, respectively, at the BLYP//MNDO level. The corresponding values for the triplet reactions (via **13t**, **15t**, and **21t**) are

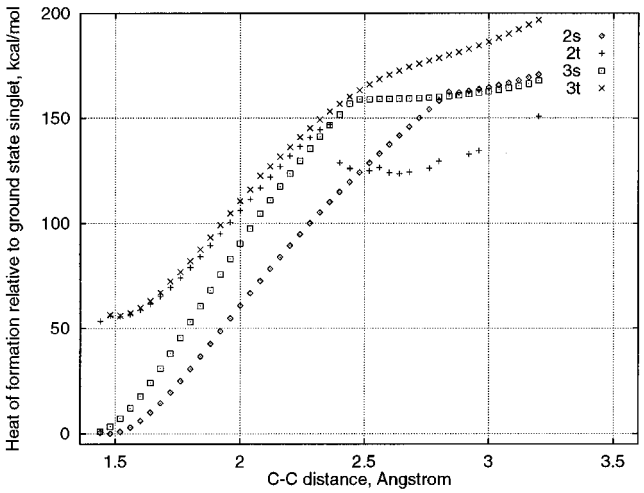

Figure 6. Opening a one-bond "window" in C_{60}. **2**: A 5−6 bond shared between a pentagon and hexagon is stretched. **3**: A 6−6 bond shared between two hexagons is stretched. Points on the **2t** triplet curve with C−C distances greater than 2.36 Å are not fully relaxed, see text.

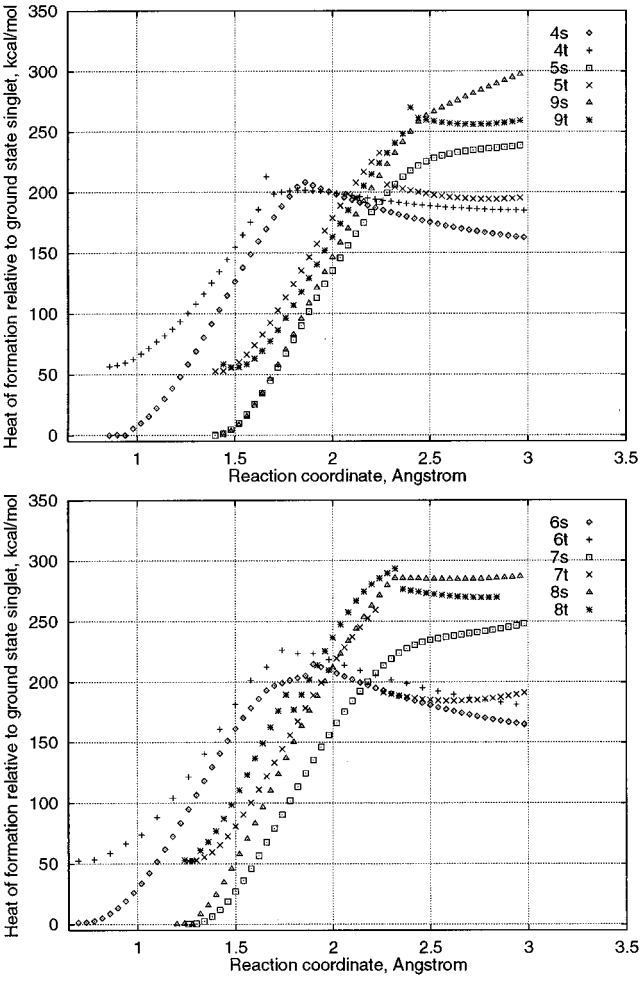

Figure 7. Opening a two-bond "window" in C_{60}. **4**: Adjacent bonds in the pentagon stretched. **5**: Nonadjacent bonds in the pentagon stretched. **6**: Adjacent bonds in the hexagon stretched. **7**: Two 5−6 bonds in the hexagon stretched. **8**: Two 6−6 bonds in the hexagon stretched. **9**: Para bonds in the hexagon stretched. Paths **9s** and **9t** are not fully relaxed, since both C−C bonds being broken were held equal along the reaction path. See Figure 1 for a definition of reaction coordinates.

even slightly higher, i.e. 262, 240, and 243 kcal/mol (BLYP//MNDO, see Table 4). The experience from the C_6H_6He reference calculations suggests that the current BLYP//MNDO approach tends to overestimate barriers, but realistic corrections would give values that are still above 200 kcal/mol. We have also checked through test calculations on **16s**, **17s**, and **21t** that the use of a polarized triple-ζ basis at helium[48] (instead of 3-21G) affects the predicted barriers only marginally, by less than 1 kcal/mol (BLYP//MNDO). None of the theoretical methods applied (MNDO, *ab initio* RHF, BLYP, BP86) yields a barriers below 225 kcal/mol for **13**−**23** (see Table 4).

In view of this situation, we have considered imperfect C_{60} isomers with the same number of formal bonds as buckminsterfullerene. There are 1812 fullerene isomers of C_{60} with pentagons and hexagons only,[49,50] and many more C_{60} isomers that contain smaller and larger rings. The simplest imperfect C_{60} fullerene isomer, containing two pairs of fused pentagons, lies within 50 kcal/mol from the perfect I_h ground state structure,[51] and is separated from the I_h structure by high barriers of more than 100 kcal/mol.[47,52] With barriers of this magnitude, imperfect C_{60} isomers should be metastable under many experimental conditions. A recent FT-Raman study of C_{60}[53] has indeed detected small amounts of C_{60} isomers with C_{2v}, D_{2h}, or D_{2d} symmetry that could not be separated from the I_h isomer by flash chromatography.

We have arbitrarily selected three "perforated" C_{60} isomers with large rings to study the insertion of helium into such metastable imperfect C_{60} species. These three isomers were required to have a classical valence structure, to contain one nine-membered or larger ring (but no three-membered ring), and to show only a localized disruption of the ideal I_h structure (in the region around the large ring). The chosen isomers **10**−**12** are given in Figure 1 (see Table 3 for relative energies), and the transition states **24**−**26** for helium insertion through the largest available ring are depicted in Figure 5 (see Table 4 for relative energies). Not surprisingly, the transition states are again more than 200 kcal/mol above the ground state I_h structure (**1s**). If such metastable "perforated" C_{60} isomers are present in a C_{60} sample as impurities, however, the effective barriers for helium insertion will refer to the energies of these metastable isomers. The resulting values (Table 5) are quite low: At the BLYP//MNDO level, helium insertion in the singlet state requires 59 kcal/mol for **24s** (through a nine-membered ring) and only 42 and 26 kcal/mol for **25s** and **26s**, respectively (through a ten-membered ring).

4. Discussion

We have investigated three mechanisms for helium incorporation into buckminsterfullerene C_{60}: The direct insertion, the one-bond window mechanism, and the two-bond window alternative. All theoretical methods applied predict barriers of more than 225 kcal/mol for each mechanism. These theoretical predictions are subject to uncertainties in the calculated geometries and energies. The barriers are based on optimized MNDO geometries which are known to be fairly accurate for stable fullerene molecules.[3] They are also expected to be reasonable for the transition structures **13**−**23** which are sterically quite constrained, so that the geometry optimization will almost be forced to put the helium atom into the

(48) Huzinaga, S. *Approximate Atomic Wavefunctions*; University of Alberta: Edmonton, 1971.
(49) Manolopoulos, D. E. *Chem. Phys. Lett.* **1992**, *192*, 330.
(50) Liu, X.; Schmalz, T. G.; Klein, D. *J. Chem. Phys. Lett.* **1992**, *192*, 331.
(51) Raghavachari, K.; Rohlfing, C. M. *J. Phys. Chem.* **1992**, *96*, 2463−2470.
(52) Yi, J. Y.; Bernholc, J. *J. Chem. Phys.* **1992**, *96*, 8634−8636.
(53) Lynch, K.; Tanke, C.; Menzel, F.; Brockner, W.; Scharff, P.; Stumpp, E. *J. Phys. Chem.* **1995**, *99*, 7985−7992.

Table 5. Effective Activation Barriers (kcal/mol) for He Insertion into Some Imperfect C_{60} Structures

label[a]	MNDO[b]	RHF//MNDO[c]	BLYP//MNDO[c]	BP86//MNDO[c]	remarks
24s	94.0	71.4	59.4	55.6	through the 9-membered ring in **10**
24t	100.8	65.3	61.1	59.9	
25s	71.2	53.0	42.1	41.5	through the 10-membered ring in **11**
25t	95.4	81.1	61.9	61.1	
26s	54.7	32.7	25.6	25.1	through the 10-membered ring in **12**
26t	81.5	52.0	49.4	49.0	

[a] s = singlet, t = triplet. [b] Optimized geometries. [c] Single-point calculations at the optimized MNDO geometries.

qualitatively correct position (see Figures 2−4). Considering the calculated energies, it is reassuring that the different theoretical approaches yield similar barriers. In the C_6H_6He reference system, the "best" theoretical methods applied to the fullerenes (BLYP/3-21G//MNDO, BP86/3-21G//MNDO) give barriers that deviate by only 6−8 kcal/mol (2−3%) from the reliable CCSD(T) reference value. Under the conservative assumption that the errors might be larger in the fullerene case by a factor of 3 (or 5), the predicted barriers would still be above 200 (or 185) kcal/mol after a corresponding correction. Hence, for the three mechanisms investigated, there can be little doubt that the barriers are of the order of 200 kcal/mol or even higher.

Barriers of this magnitude are compatible with the high-energy collision experiments since the available kinetic energy in the center-of-mass coordinate system is sufficient to overcome such barriers. Under different experimental conditions (sample preparation, temperature) the observed threshold energy for helium capture by C_{60}^- anions varies strongly in the collision experiments:[16] It is about 8 eV for cold C_{60}^-, about 6 eV under standard conditions (around 2000 K, internal energy of the molecule approximately 30 eV), and as low as 3 eV for "much hotter" C_{60}^-. Molecular dynamics simulations[54] indicate that there is a gradual onset of a "floppy phase" of C_{60} at a temperature of 2400 K, with substantial cluster shape deformations. Consequently the lowest observed threshold energies for the hottest C_{60}^- sample (3 eV) have been associated with imperfect fullerene structures that have defects (large holes) in their cages.[16] This interpretation is consistent with our present theoretical results for imperfect isomers (see Table 5, 3 eV ≈ 70 kcal/mol).

The observation of helium incorporation into C_{60} and of helium release from $He@C_{60}$ under thermal conditions[8−10] cannot be reconciled with the exceedingly high barriers that we have computed for helium passage through the buckminsterfullerene cage. In particular, our calculations would seem to exclude the possibility that helium release from $He@C_{60}$ with an apparent barrier around 80 kcal/mol[8] proceeds by any of the three mechanisms studied (see above). The low barrier reported must be attributable to effects of impurities.[55] We suggest an experimental reinvestigation using highly purified material.

Considering the high-pressure experiments on helium incorporation under thermal conditions,[9,10] it is instructive to estimate the expected yield of $He@C_{60}$ at equilibrium. For this purpose we have adopted the simple model[8] that the average number of helium atoms per C_{60} molecule (equivalent to the percentage of filled C_{60} cages) is obtained by multiplying the helium concentration in the gas (assumed to be ideal) with the accessible volume per cage. Rather than using a hard-sphere approach[8,9] we have determined the accessible volume from quantum-chemical data: Assuming the potential to be isotropic inside the cage[3] we have evaluated its radial dependence by moving He along the C_5 axis in $He@C_{60}$ and employed the calculated

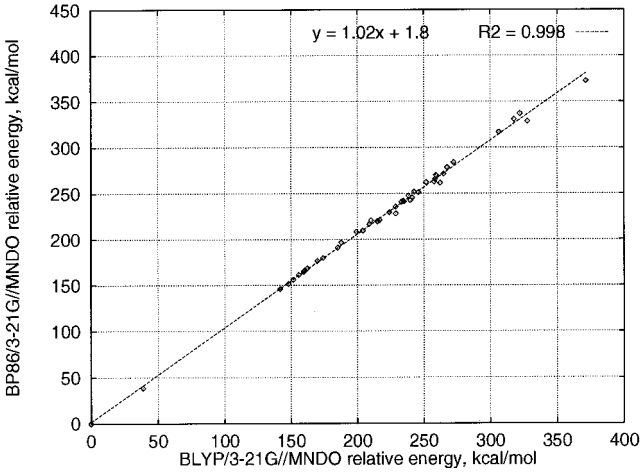

Figure 8. Correlation between relative energies of C_{60} and $C_{60}He$ structures computed at the BP86/3-21G//MNDO and BLYP/3-21G//MNDO levels. The average signed and unsigned errors with respect to BLYP/3-21G//MNDO are 6.2 and 6.3 kcal/mol, respectively.

energies for defining Boltzmann weight factors in an integration over the volume of the cage. At typical experimental conditions (e.g. T = 900 K, p = 2000 atm)[9,10] this procedure yields an accessible volume of 2.8−3.1 Å^3 and thus an effectively accessible spherical region with a radius of about 0.9 Å in C_{60} (*ab initio* RHF/3-21G, BLYP/3-21G), in reasonable agreement with previous estimates.[8] This leads to the prediction that about 4−5% of the C_{60} cages should be filled with helium under typical experimental conditions (see above) if thermodynamic equilibrium were achieved. The observed yield of $He@C_{60}$, however, is only around 0.1%.[9,10] Two conclusions emerge from these findings: First, an equilibrium distribution of helium inside and outside the buckminsterfullerene cages has apparently not yet been reached after 5 h at high temperature and pressure,[9,10] which may be taken as evidence against a low-barrier insertion process involving only helium and buckminsterfullerene. Second, if there is another species with a similar accessible volume in equilibrium with helium, a few percent of such an impurity would be sufficient to arrive at the observed yield of 0.1%. Hence, if the fullerene material used in the experiment would contain this percentage of metastable imperfect C_{60} isomers with larger rings, helium insertion could be feasible due to the much lower barriers (see Table 5). However, this mechanistic alternative would require an annealing of the imperfect cage to buckminsterfullerene during the course of the high-pressure experiment because the product $He@C_{60}$ has been shown by ^{13}C -NMR spectroscopy to contain the buckminsterfullerene cage.[10] In view of the high barriers calculated for annealing processes[47,52] this mechanism does not seem very likely. It may be checked experimentally by carrying out the high-pressure experiment with the usual fullerene material first in an inert N_2 atmosphere (allowing for possible annealing, no N_2 incorporation) and using the resulting material in a high-

(54) Kim, S. G.; Tománek, D. *Phys. Rev. Lett.* **1994**, *72*, 2418−2421.
(55) Saunders, M. Private communication, **1996.**

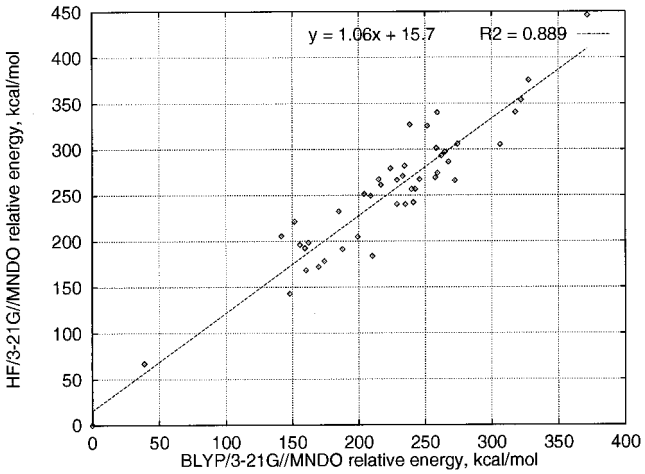

Figure 9. Correlation between relative energies of C_{60} and $C_{60}He$ structures computed at the HF/3-21G//MNDO and BLYP/3-21G//MNDO levels. The average signed and unsigned errors with respect to BLYP/3-21G//MNDO are 30 and 31 kcal/mol, respectively.

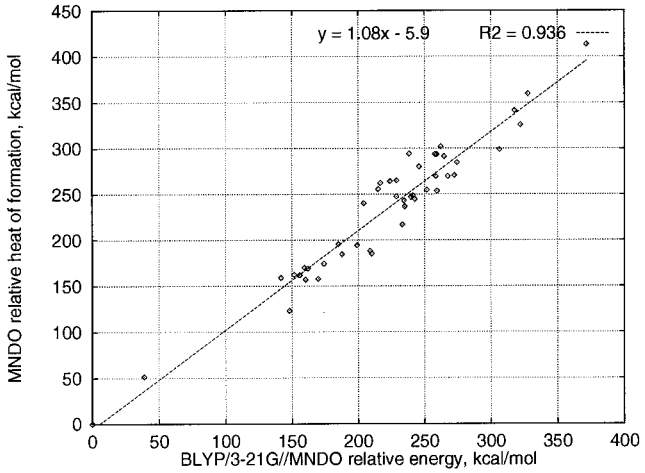

Figure 10. Correlation between relative energies of C_{60} and $C_{60}He$ structures computed at the MNDO and BLYP/3-21G//MNDO levels. The average signed and unsigned errors with respect to BLYP/3-21G//MNDO are 12 and 18 kcal/mol, respectively.

pressure experiment with helium: The yield of $He@C_{60}$ should then be much reduced if insertion occurs through imperfect C_{60} isomers.

Another mechanistic alternative involves impurities which add to the fullerene, thereby weakening the bonds in the cage and allowing an easier incorporation of helium (through one of the pathways studied presently for C_{60}). This mechanism which has also been considered by others[55] seems plausible since addition and elimination are sometimes found to be reversible in fullerene chemistry. Hence, $He@C_{60}$ could be generated from an intermediate $He@C_{60}X$ by eliminating the impurity (X) again. We have started some preliminary calculations on such processes but it is too early to report on the results.

Our final topic concerns a computational issue. Having calculated many unusual fullerene species at different theoretical levels (see Tables 1, 3, and 4), it seems worthwhile to investigate the consistency of the computational results by a statistical analysis of relative energies (evaluated at optimized MNDO geometries). We have chosen the BLYP/3-21G//MNDO energies as reference data and performed a linear regression analysis for the BP86/3−21G//MNDO, *ab initio* HF/3-21G//MNDO, and MNDO energies. The results are shown in Figures 8−10. Not surprisingly, the correlation is best for the two DFT approaches (BP86 vs BLYP, Figure 8), with a correlation coefficient of 0.998. There are no outliers in this correlation indicating that the failure of BLYP for the C_{20} isomers[29,30] probably represents an exceptional case for fullerene chemistry. Judging from Figures 9 and 10, MNDO is superior to *ab initio* HF/3-21G in reproducing the BLYP/3-21G reference data, both in terms of the average errors and the correlation coefficients (0.936 vs 0.889). Hence, when attempting to improve on MNDO results for fullerenes, it may often be best to move directly to correlated theoretical treatments (DFT or *ab initio*).

5. Conclusions

According to our MNDO, *ab initio* SCF, and DFT results, the incorporation of helium into C_{60} must overcome a barrier of more than 200 kcal/mol relative to non-interacting ground-state buckminsterfullerene and helium, regardless of the actual mechanistic pathway on the potential $C_{60}He$ surface. Hence, the formation of $He@C_{60}$ under thermal conditions cannot proceed in a single kinetic step, but must involve intermediates. The window-type structures considered are probably not the required intermediates since they do not seem to be stable enough kinetically. Mechanistic alternatives may include insertion of helium into metastable C_{60} isomers as well as catalytic processes involving impurities in C_{60} and on the surface of the reaction vessel. Further experimental and theoretical work is needed to investigate these possibilities.

Acknowledgment. This work was supported by the Schweizerischer Nationalfonds. Parts of the computations were performed at the Competence Center for Computational Chemistry at ETH Zürich.

JA9607695

(56) Bacskay, G. B. *Chem. Phys.* **1981**, *61*, 385−404.

(57) Cartesian coordinates for all structures are available from the authors on request.